Chapter 4.1

Shared Synaptic Pathophysiology in Syndromic and Non-syndromic Rodent Models of Autism

Stéphane J. Baudouin, Julien Gaudias, Stefan Gerharz, Laetitia Hatstatt, Kuikui Zhou, Pradeep Punnakkal, Kenji F. Tanaka, Will Spooren, Rene Hen, Chris I. De Zeeuw, Kaspar Vogt, Peter Scheiffele

Abstract

The genetic heterogeneity of autism poses a major challenge for identifying mechanism-based treatments. A number of rare mutations are associated with autism, and it is unclear whether these result in common neuronal alterations. Monogenic syndromes, such as Fragile X, include autism as one of their multi-facetted symptoms and have revealed specific defects in synaptic plasticity. We discovered an unexpected convergence of synaptic pathophysiology in a non-syndromic form of autism with those in Fragile X syndrome. Neuroligin-3 knock-out mice (a model for non-syndromic autism) exhibited disrupted hetero-synaptic competition and perturbed metabotropic glutamate receptor-dependent synaptic plasticity, a hallmark of Fragile X. These phenotypes could be rescued by re-expression of neuroligin-3 in juvenile mice, highlighting the possibility for reverting neuronal circuit alterations in autism after completion of development.

Autism comprises a heterogeneous group of neurodevelopmental disorders characterized by variations in social interactions, communication, and the manifestation of ritualistic behaviors (1). A large number of rare high-impact mutations have been identified in autistic patients (2-4). However, most insights into the synaptic pathophysiology of autism are derived from models of monogenic syndromes, such as Fragile X Syndrome, where about 25% of patients meet diagnostic criteria of autism (5). In Fragile X, the key defect in synaptic transmission is elevated group I metabotropic glutamate receptor-dependent synaptic plasticity (mGluR-LTD). However, most cases of autism are non-syndromic, and it is unclear whether these share pathophysiology with Fragile X. One class of non-syndromic forms of autism is associated with mutations in the Neuroligin genes (Nlgn1,2,3,4), which encode postsynaptic adhesion molecules involved in synapse assembly (proteins NL1,2,3,4) (6-8). For Nlgn3, a R451C point mutation (7) and deletions (4, 9) have been identified in several patients with autism. The R451C point mutation results in NL3 trafficking defects (10) whereas the deletions remove the entire Nlgn3 coding sequence (4, 9). Nlgn3 ^{R451C} knock-in and Nlgn3^{KO} mice exhibit impairments in social interactions, social memory, ultrasonic vocalization, and olfaction (11, 12 but see 13). For Nlgn3^{R451C}, synaptic transmission is altered in somatosensory cortex and hippocampus (12, 14). However, the subcellular localization of NL3 protein in vivo and synaptic defects resulting from Nlgn3 ablation are unclear (15, 16). To understand the pathophysiology of Nlgn3 deletions, we focused on the synaptic connectivity in the cerebellum because cerebellar activation is altered in autistic patients (17) and cerebellar lesions result in behavioral changes reminiscent of autism (18,

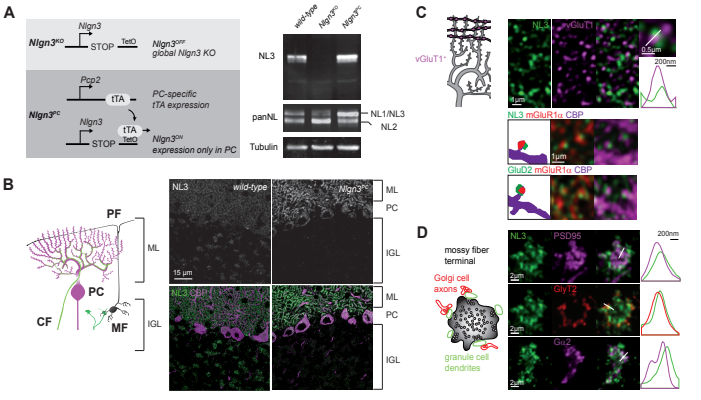

Fig. 1: Cell-type specific synaptic localization of NL3

(A) Nlgn3^{KO} (Nlgn3$^{STOP\text{-}tetO}$) mice lack NL3 protein expression and Nlgn3^{PC} mice (Nlgn3$^{STOP\text{-}tetO}$::Pcp2^{tTA}) show re-expression in cerebellar lysates. (B) Mossy fiber inputs (MF) in the inner granular layer (IGL) are relayed to PCs via parallel fibers (PF). Climbing fibers (CF) form synapses directly onto the proximal PC dendritic arborization. In Nlgn3^{PC} mice NL3 immunoreactivity is increased on PC dendrites (calbindin, CBP) and abolished in IGL. (C) NL3 is apposed to vGluT1^{+} PF boutons and colocalizes with mGluR1α in CBP^{+} spines, similar to GluD2. (D) In glomeruli, NL3 is detected at PSD95^{+} and GABA-A receptor α2^{+} synapses, and colocalizes with GFP^{+} terminals in GlyT2^{GFP} transgenic mice.

19). Using NL3-specific antibodies (16) we detected strong NL3-immune-reactivity in the molecular layer and surrounding mossy fiber glomeruli of the inner granular layer (Fig. 1A,B). Antibody-reactivity was largely abolished in mutant mice carrying a STOP cassette inserted after the transcriptional start site (20) which resulted in a complete loss of NL3 expression (Nlgn3^{KO}) (Fig. 1A,S1A,B). In the inner granular layer, NL3 was detected at glutamatergic as well as GABAergic synapses whereas NL3 in the molecular layer was primarily detected at parallel fiber synapses (Fig. 1C,D). In the same preparations, we detected only little apposition of NL3 immune-reactivity with markers of climbing fiber and interneuron synapses (Fig. S1C). Similar observations were made in Nlgn3^{PC} mice, a knock-out allele where NL3 is selectively re-expressed in Purkinje cells under control of the tetracycline-transactivator (Fig. 1A,B,S1D).

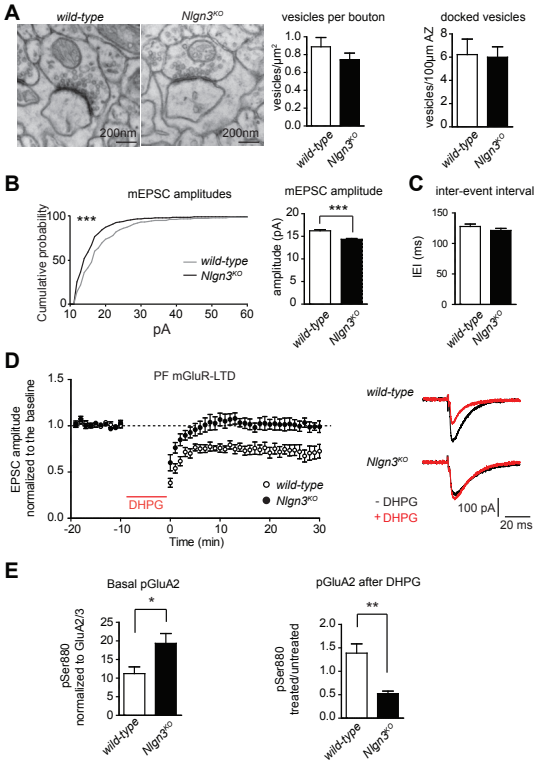

Fig. 2: Occlusion of mGluR-LTD in Nlgn3^{KO}

(A) PF synaptic ultrastructure in Nlgn3^{KO} by transmission electron microscopy (n≥4 animals, 200 synapses / animal).

(B) Cumulative distribution of mEPSCs (***p < 0.001 Kolmogorov-Smirnov test) and mean amplitude (n = 9 cells for wild-type and n = 21 for Nlgn3^{KO}, ***p < 0.001 Mann-Withney).

(C) mEPSC inter-event intervals, paired pulse ratios (n = 9 wild-type and n = 15 Nlgn3^{KO}).

(D) mGluR-LTD induced by 10 min 50 μM DHPG (n ≥ 8 cells) and representative traces before (black) and after (red) DHPG stimulation.

(E) Quantitative western blot of basal and DHPG-induced phospho-GluA2 (normalized to GluA2/3 protein level, n ≥ 4 mice, *p < 0.03, t-test). DHPG-induced phosphorylation expressed as ratio for treated to untreated samples (n ≥ 4 mice, **p < 0.01, t-test).

Ultrastructural analysis of parallel fiber synapses in Nlgn3^{KO} mice did not reveal a dramatic difference in several morphological parameters (Fig. 2A). mEPSC recordings in Nlgn3^{KO} Purkinje cells identified a small but significant reduction in mEPSC amplitude (Fig. 2B) whereas paired-pulse facilitation of parallel fiber synapses was not detectably altered (Fig. 2C,S2A). Parallel fiber synapses exhibit a marked long-term depression that is thought to contribute to forms of cerebellar function and learning (21 but see 22). Simultaneous activation of group I mGluRs and AMPA receptors in the postsynaptic compartment results in PKC-activation, AMPA receptor (GluA2 subunit) phosphorylation at Serine 880 and subsequent dissociation from the postsynaptic scaffold and endocytosis (21, 23). Given the reduction in mEPSC amplitudes, we tested whether mGluR-dependent LTD was modified in Nlgn3^{KO} Purkinje cells. In 2-3 months old wild-type mice, application of the group I mGluR agonist DHPG resulted in a persistent reduction of EPSC amplitudes. No depression was observed in Nlgn3^{KO} cerebellar slices (Fig. 2D,S2B). This loss in mGluR-LTD may be a consequence of an impaired LTD-expression or an occlusion due to constitutive activation. We observed a two-fold increase in basal GluA2-phosphorylation at Serine 880 in Nlgn3^{KO} as compared to wild-type. Upon

DHPG stimulation, phospho-GluA2 levels were increased in wild-type but decreased in Nlgn3^{KO}, likely due to mGluR-stimulated degradation of the phosphorylated form of GluA2 (Fig. 2E) (24).

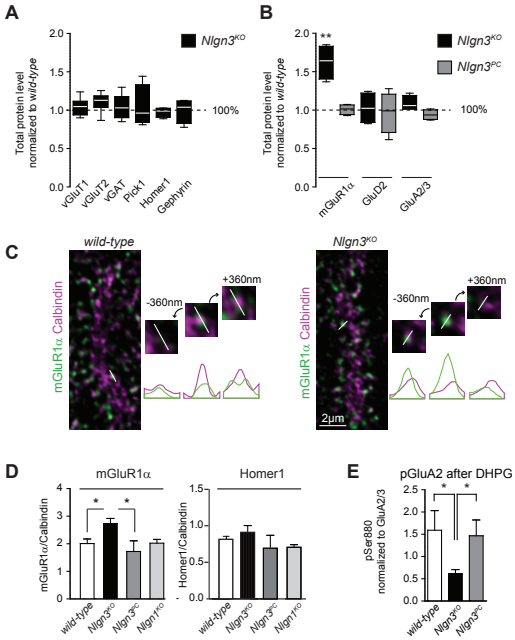

Fig. 3: Elevation of synaptic mGluR1 levels in Nlgn3^{KO} mice
(A) Quantitative western blot, protein levels were normalized to tubulin and expressed relative to wild-type.
(B) Quantitative western blot of mGluR1α, GluD2, and GluA2/3 levels in cerebellum (normalized to tubulin and expressed relative to wild-type, n ≥ 4, ** p = 0.002, t-test).
(C) Quantitative line scan on cerebellar sections stained with anti-mGluR1α, anti-Homer 1, and anti-Calbindin antibodies.
(D) Line scan intensity ratios of mGluR1α/CBP and Homer1/CBP (n = 6 mice, 1200 synapses / genotype; mGluR1α *p = 0.04, Homer p = 0.6, t-test). Re-expression of NL3 in PC restores mGluR1α level (n = 4 mice, p = 0.4). No difference in Nlgn1^{KO} mice (n = 6 mice, p = 0.9).
(E) DHPG-induced phosphorylation of GluA2 expressed as ratio for treated to untreated samples (normalized to GluA2/3 protein level, n ≥ 5 mice, * p < 0.05, t-test).

The constitutive increase in phospho-GluA2 in Nlgn3^{KO} cerebellum indicated a gain-of-function in the synaptic plasticity pathway. Parallel fiber-LTD is regulated by several postsynaptic receptors, including GluA2, GluD2, and mGluR1α (21). Using quantitative western blotting we discovered a selective increase in the mGluR1α protein in Nlgn3^{KO} cerebellum whereas the mRNA level was unchanged (Fig. 3A,B, S3, note similar mGluR1α protein increase in thalamus). mGluR2 and mGluR7, two additional metabotropic receptors expressed in the cerebellum were unaltered (Fig.S3B). Endogenous mGluR1 and NL3 co-localized in the heads of Purkinje dendritic spines (Fig.1D). In Nlgn3^{KO} synaptic mGluR1 levels were increased but unaltered in Nlgn1^{KO} cerebellum (Fig. 3C,D). This mGluR1α de-regulation was a cell autonomous consequence of NL3 loss-of-function because re-expression of NL3 specifically in Purkinje cells (Nlgn3^{PC}) reduced the mGluR1α protein level and its synaptic abundance back to wild-type level (Fig. 3B,D). Moreover, DHPG-induced phospho-GluA2 signals were returned to wild-type levels in mice that selectively re-express NL3 protein in Purkinje cells (Nlgn3^{PC}, Fig.3E).

We next examined whether loss of NL3 results in wiring alterations in the cerebellar network. In the mature cerebellum, each Purkinje cell is innervated by a single climbing fiber, and synaptic competition between parallel fiber and climbing fiber inputs excludes climbing fiber inputs from the Purkinje cell distal dendrites (21, 25). In Nlgn3^{KO} cerebella we observed a significant invasion of vGluT2^{+} terminals into the distal molecular layer (Fig. 4A,B, Fig.S4A). Ectopic climbing fiber synapses were not observed in Nlgn1^{KO} cerebella and expression of Nlgn3 exclusively in Purkinje cells was sufficient to suppress ectopic synapse formation in Nlgn3^{PC} mice. Synapse density along the entire length of the overshooting climbing fibers was unaltered, resulting in an increased total number of climbing fiber synapses (Fig. 4A and B, Fig. S4A). Consistent with this observation, evoked climbing fiber transmission was elevated in the Nlgn3^{KO} mice (Fig. 4C, note normal regression of multi-innervation, Fig. S4B).

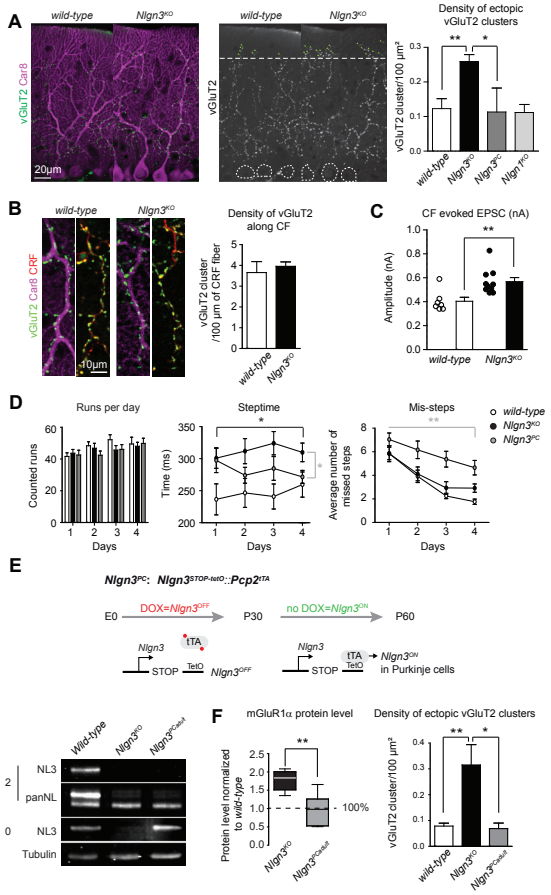

Fig. 4: Disrupted hetero-synaptic competition and adult phenotypic rescue in Nlgn3^{KO} mice

(A) vGluT2 puncta on distal PC dendritic tree (upper 20%, dashed line, anti-carbonic anhydrase-related protein VIII, Car8) marked by green arrowheads (vGluT2$^+$ clusters/100μm^2, n=6 mice per genotype, **p = 0.0023 for wild-type vs. Nlgn3^{KO}, t-test).

(B) Density of CF synapses along individual fibers (CRF$^+$, n ≥ 3 mice, p = 0.6).

(C) Evoked CF-PC transmission assessed by extracellular stimulation (n ≥ 7 cells from ≥ 4 mice, **p = 0.003, t-test).

(D) Counted runs, Steptimes and missed steps on Erasmus Ladder (n ≥ 10, *p < 0.05, **p < 0.01, ANOVA, post hoc Tukey test). Performance of Nlgn3^{PC} mice over four training days is indistinguishable from wild-type (p = 0.2, ANOVA, post hoc Tukey test).

(E) Adult re-expression of NL3. Doxycycline (100μg/ml from E0) removed at P30, mice sacrificed at P60.

(F) Quantitative western blot of mGluR1α in Nlgn3^{PCadult} mice (P60, n ≥ 5 mice, **p = 0.004).

We used the Erasmus Ladder (26) to explore motor coordination in Nlgn3^{KO} mice. In this behavioral assay, mice cross a ladder consisting of pressure sensors measuring motor output. Wild-type and Nlgn3^{KO} mice completed the same number of valid runs on the ladder. Steptimes for Nlgn3^{KO} mice were significantly elevated, indicating a perturbation of motor coordination (Fig. 4D). The occurrence of mis-steps during ladder crossing was unaltered in the Nlgn3^{KO} mice and declined similarly as for wild-type over several days of training. NL3 expression specifically in Purkinje cells rescued the elevated step times progressively after several training days (Fig. 4D). Notably, Nlgn3^{PC} mice did exhibit a higher number of mis-steps (Fig. 4D), most likely because the re-expression in Purkinje cells exceeds the endogenous NL3 level and results in a gain-of-function phenotype.

The extensive ectopic synapse formation in Nlgn3^{KO} mice raises the question whether such structural defects can be corrected after the completion of development. We used the tetracycline-transactivator to temporally control the re-expression of NL3 in PCs of Nlgn3^{PC} mice (Fig. 4E). Nlgn3^{PC} mice were raised in the presence of doxycycline (transactivator inactive, NL3 expression off, Fig. 4E). At P30, doxycycline was removed, permitting re-expression of NL3 selectively in Purkinje cells. Strikingly, re-expression restored wild-type mGluR1α protein levels and resulted in the removal of ectopic synapses from the distal Purkinje cell dendritic tree (Fig. 4F, Fig. S4C, D). Therefore, neurodevelopmental phenotypes and ectopic synapse formation arising from Nlgn3 deletion can be corrected in the mature cerebellar system.

Our results provide insight into the synaptic pathophysiology of a model of non-syndromic autism. Phenotypes observed in Nlgn3^{KO} mice represent a surprising parallel to the synaptic pathophysiology in Fmr1 and Tsc2 mutant mice (27). Like these syndromic autism models, Nlgn3^{KO} mice exhibit a de-regulation of mGluR-LTD. In the Fmr1^{KO} mice mGluR-LTD in forebrain and cerebellar neurons is increased, and this phenotype can be suppressed by reduction of group I mGluR activity (5, 28, 29). Nlgn3^{KO} mice exhibit an occlusion in mGluR-LTD due to increased mGluR1α expression, indicating a common core pathway of synaptic dysfunction. mGluR5 antagonists can revert cellular phenotypes in Fmr1^{KO} mice and may show therapeutic benefit in some Fragile X patients (5, 30). Our work indicates that group I mGluR antagonists hold promise for designing treatment strategies for non-syndromic autism. Our genetic experiments in Nlgn3^{KO} mice reveal that not only functional alterations but also ectopic synapse formation can be reversed, highlighting that structural neurodevelopmental phenotypes can be rescued by intervention after the completion of development.

References and Notes

1. American Psychiatric Association Task Force On DSM-IV, Diagnostic and statistical manual of mental disorders: DSM-IVTR. A. P. Association, Ed., (2000).
2. R. Toro et al., Trends Genet. 26, 363 (2010).
3. D. Levy et al., Neuron 70, 886 (2011).
4. S. J. Sanders et al., Neuron 70, 863 (2011).
5. H. Y. Zoghbi, M. F. Bear, Cold Spring Harbor Perspectives in Biology 4, (2012).
6. T. C. Sudhof, Nature 455, 903 (2008).
7. S. Jamain et al., Nature Genetics 34, 27 (2003).
8. B. Chih, H. Engelman, P. Scheiffele, Science 307, 1324 (2005).
9. S. R. Gilman et al., Neuron 70, 898 (2011).
10. B. Chih, S. K. Afridi, L. Clark, P. Scheiffele, Hum. Mol. Genet. 13, 1471 (2004).
11. K. Radyushkin et al., Genes Brain Behav. 8, 416 (2009).
12. K. Tabuchi et al., Science 318, 71 (2007).
13. K. K. Chadman et al., Autism Res. 1, 147 (2008).
14. M. Etherton et al., Proc. Natl. Acad. Sci. USA 108, 13764 (2011).
15. F. Varoqueaux et al., Neuron 51, 741 (2006).
16. E. C. Budreck, P. Scheiffele, Eur. J. Neurosci. 26, 1738 (2007).
17. S. H. Mostofsky et al., Brain 132, 2413 (2009).
18. J. D. Schmahmann, J. B. Weilburg, J. C. Sherman, Cerebellum 6, 254 (2007).
19. P. T. Tsai et al., Nature, (2012).
20. K. F. Tanaka et al., Biol. Psychiatry 67, 770 (2010).
21. M. Kano, K. Hashimoto, T. Tabata, Philosophical Transactions of the Royal Society of London 363, 2173 (2008).
22. M. Schonewille et al., Neuron 70, 43 (2011).
23. J. P. Steinberg et al., Neuron 49, 845 (2006).
24. A. M. Mabb, M. D. Ehlers, Annu. Rev. Cell Dev. Biol. 26, 179 (2010).
25. R. Cesa, P. Strata, Neuroscience 162, 624 (2009).
26. R. S. Van Der Giessen et al., Neuron 58, 599 (2008).
27. B. D. Auerbach, E. K. Osterweil, M. F. Bear, Nature 480, 63 (2011).
28. S. K. Koekkoek et al., Neuron 47, 339 (2005).
29. C. Luscher, K. M. Huber, Neuron 65, 445 (2010).
30. S. Jacquemont et al., Science Translational Medicine 3, 64ra1 (2011).

Materials and Methods

Animals. GlyT2^{GFP}, Nlgn1^{KO}, Nlgn3^{KO} and Pcp2^{tTA} mice were previously described (1-4) and were maintained in C57/Bl6 background. All mice used for analysis were males between 2 and 3 months old, except for the recording of PF mEPSCs (Figure 2B,C) and pGluA2 analysis in Figure 3E where mice were between postnatal day 21 and 28. Mice had free access to standard laboratory food and water and were maintained on a 12h light/dark cycle. When desired, doxycycline 100μg/ml was added to the drinking water during breeding and after weaning of pups. Subsequently, doxycycline was removed to allow for Nlgn3 re-expression.

Antibodies, qPCR assays. Affinity-purified anti-NL1, 2, 3 isoform-specific antibodies, anti-panNL antibodies (5, 6), guinea-pig anti-GABA A α2 (7, kind gift from J.M. Fritschy), rabbit anti-GluA2/3 (8, kind gift from Nathalie Sans) were previously described. The following commercially available antibodies were used: guinea-pig anti-vGluT1 (Chemicon), mouse-vGluT2 (Chemicon), rabbit anti-vGAT (Synaptic Systems), mouse anti-PSD95 (ABR), mouse anti-Calbindin (Swant), mouse anti-vGluT1 (Synaptic Systems), mouse anti-Pick1 (NeuroMab), rat anti-Homer1 (Chemicon), mouse anti-gephyrin (Synaptic systems), rabbit anti-phospho Ser880 GluA2 (Chemicon), rabbit anti-GluD2 (Frontier Institute), goat anti-mGluR1α (Frontier Institute), mGluR2 (Abcam), mGluR7 (Abnova), rabbit anti-Homer1 (Chemicon), goat anti-Car8 (Frontier Institute), rabbit anti-Corticotropin-Releasing Factor (Peninsula Laboratories).

Total RNA was isolated using Trizol reagent (Invitrogen), followed by removal of contaminating DNA using Turbo DNA-free (RNase-free DNase; Ambion). 1 μg of total RNA was reverse transcribed using random hexamers and Superscript III (Invitrogen). Taqman® gene expression assays (Applied Biosystems) were performed following manufacturers' instructions using the following probes: Mm00810231_s1 for Grm1 (protein mGluR1), Mm01235831_m1 for Grm2 (protein mGluR2), Mm00690332_m1 for Grm5 (protein mGluR5), Mm01189424_m1 for Grm7 (protein mGluR7) and Mm99999915_g1 for Gapdh.

Immunohistochemistry, Image Acquisition, Imagepost-treatment and Analysis. All experiments were performed blind with respect to the genotype. For each experimental series, all images were acquired in the same imaging session with identical settings for laser power, photomultiplier or EM-CCD camera gain and offset. For localization of endogenous NL3, tissue was prepared following an advanced live sectioning protocol (9). Briefly, mice were sacrificed by CO_2 inhalation, the cerebellum dissected and rapidly placed in a vibratome chamber and sectioned at 300μm in cold oxygenated aCSF (in mM: 125 NaCl, 2.5 KCl, 1 $MgCl_2$, 2 $CaCl_2$, 1.25 NaH_2PO_4, 20 Glc, 26 $NaHCO_3$, 95% O_2/5% CO_2). Slices obtained were maintained at 33°C for 30 min in oxygenated aCSF, fixed 20 min in 4% PFA in PBS and incubated in 30% sucrose in PBS overnight. Ten micrometers sections were obtained using a cryostat, directly mounted on coverglass and stored at -20°C. Prior to staining sections were dried at room-temperature for 1h and rehydrated for 15 min in 50 mM Tris-HCl/ 150 mM NaCl pH7.4 with 0.05% Triton. Sections were then immunostained using standard procedures.

For quantitative line scan analysis and the analysis of climbing fiber synapse density, sections were obtained after transcardial perfusion with fixative (4% paraformaldehyde/15% picric acid in 100 mM phosphate buffer, pH 7.2). Tissues were sectioned at 30 μm on a cryostat and floating sections were immunostained following standard procedures.

Image acquisition for quantitative line scan analysis and the localization of NL3 was on a confocal microscope with a 63x/1.4 NA oil objective at a pixel size of 93 nm and optical sections of 370 nm. Image resolution was 1024x1024 pixels with a data depth of 12 bits. Images were processed by

deconvolution using a theoretical PSF, a signal/noise ratio of 15 for each channel and 30 iterations of the deconvolution algorithm. Direct apposition of cellular markers was identified using a three-dimensional line scan tool.

For the analysis of climbing fiber synapse density, images were acquired on a LIS-spinning disk confocal system (40x/1.3 NA objective, 0.4 μm optical sections). Four separate fields were acquired in two separate cerebellar sections per animal in the straight portion of lobule IV/V, where the PC dendritic arborization is exactly aligned with the parasagittal plane. Density of CF terminals was analyzed with Metamorph (Molecular Devices). Five optical planes were chosen based on the Purkinje cell marker Car8. The thickness of the molecular layer was measured from the distal part to the most proximal dendritic portion from the Purkinje cell body. The most distal fifth of the molecular layer was selected and the vGluT2 clusters isolated based on a manual thresholding. The number of vGluT2 clusters was normalized to the recorded area. The density of vGluT2 clusters along individual CF was analyzed in 3D. Corticotropin-Releasing Factor was used to label CF in the lobule X of the cerebellum. CRF^{+} fibers were traced within the entire molecular layer, clusters were manually recorded, and cluster number was normalized to CF length.

Three-dimensional line scan analysis was performed using point measurement plugin software. Each line scan was drawn on a single optical section on a PF synapse identified as labeled with Calbindin, Homer1 and mGluR1α. For each synapse the same line scan was transfered on the adjacent optical sections directly above and below. The intensity curve for each line scan was extracted using Matlab software. The intensity was recorded as the integral of the intensity curve minus the local background using custom software (developed by A. Ponti, Friedrich Miescher Institute, Basel, Switzerland). The intensity of three optical planes for each channel was summed up and the intensity for mGluR1 and Homer1 expressed was normalized to the Calbindin intensity in the same planes. Images were assembled using Adobe Photoshop and Illustrator Software.

Biochemistry. For analysis of the phosphorylation of GluA2 serine 880 (pSer880) analysis, 300 μm vibratome slices of the cerebellum (see immunohistochemistry for details) were treated with 50 μM (S)-3,5-Dihydroxyphenylglycine (DHPG) or with vehicle (aCSF) for 10 min then snap frozen in liquid nitrogen. Sections were lysed in Laemmli Buffer (50 mM Tris-HCl, pH6.8, 100mM DTT, 2% SDS, 10% glycerol) and 25 μg protein was separated by polyacrylamide gel electrophoresis and transferred onto nitrocellulose membrane. Blots were blocked in Tris-buffered saline containing 5% milk powder. For visualization of pSer880 horseradish peroxidase (HRP)-conjugated secondary antibody and enhanced chemoluminescent detection were used. Signals were acquired using a CCD camera. The membrane was subsequently blocked in Tris-buffered saline containing 3% Top Block. Relative GluA2/3 protein expression was determined using IRDye coupled secondary antibodies and quantified and level of pSer880 normalized to GluA2/3 protein.

For analysis of cerebellar protein, cerebella were lysed in 25 mM Tris-HCl, 150 mM NaCl, 1% Triton, 0.2% SDS, 5mM EDTA, 2mM DTT, 1mM NaF, 1mM Na_3VO_4 containing protease inhibitor cocktail. The soluble fractions were analyzed by immunoblotting with primary antibodies for 24 hrs at 4°C. Twenty-five micrograms of protein were separated by polyacrylamide gel electrophoresis and transferred on nitrocellulose. Blots were blocked in Tris-buffered saline containing 3% Top Block. Relative protein expression was determined using IRDye coupled secondary antibodies. Fluorescence images were acquired and quantified and were normalized to Tubulin.

Electron microscopy. Animals were transcardially perfused with fixative (2% paraformaldehyde/2% glutaraldehyde in 100 mM phosphate buffer, pH 7.4). Tissues were sectioned at 60 μm in PBS on

a vibratome. Sections were washed in 0.1M cacodylate buffer, pH7.4, postfixed in 0.1M reduced osmium (1.5% $K_4Fe(CN)_6$, 1% OsO_4 in water) and embedded in Epon resin. Images were acquired on a Transmission Electron Microscope. Quantification of the number of vesicles was performed using XtraCount software (developed by C. Olendrowitz, Göttingen, Germany).

Electrophysiological recordings. Male mice (experimenter blind to genotype) were deeply anesthetized by Isoflurane® inhalation, cerebella were quickly removed and placed in ice-cold aCSF (in mM: 125 NaCl, 5 KCl, 1 $MgCl_2$, 2 $CaCl_2$, 1.25 NaH_2PO_4, 20 Glc, 26 $NaHCO_3$). Two hundred fifty micron parasagittal sections for CF innervation and mGluR-LTD recordings or coronal sections for spontaneous mEPSC recordings were obtained using a vibrating blade microtome. Slices were placed in room temperature oxygenated aCSF to recover for one hour, then placed in an incubation chamber of an upright microscope equipped with a 20 x lens and superfused at room temperature with oxygenated aCSF at a rate of 1 ml/min. Slices were illuminated using a custom-built IR LED system. Purkinje cells were visualized using Nomarski interference contrast and the image captured with an IR-sensitive video camera.

Whole-cell patch-clamp recordings (pipette resistance=2-4MΩ) were obtained from Purkinje cells using Cs-based internal solution (in mM: 130 Cs-Methane-Sulfonate, 5 CsCl, 5 EGTA, 10 HEPES, 1 Mg-ATP, 0.1 Na-GTP, pH 7.31, 291mOsm) for CF stimulation or for mEPSC recordings and K-based internal solution (in mM: 120 K-Gluconate, 5 KCl, 11 tris-Phosphocreatine, 20 HEPES, 4.5 Mg-ATP, 0.3 Tris-GTP, 1 EGTA, pH=7.3, 291mOsm) for mGluR-LTD experiments. Signals were recorded using a dual voltage- and current-clamp amplifier. Data was filtered at 10 kHz and digitized at 20 kHz using an A/D board using custom-written macros.

For CF stimulation (mice 2-3 months of age), cells were voltage-clamped at +20 mV to minimize driving force and avoid spurious activation of voltage gated conductances. A patch pipette (1MΩ) filled with aCSF was placed in the granular cell layer, in the vicinity of the PC, and moved until the climbing fiber response could be elicited with a minimal stimulus intensity. Two current pulses (0.1ms, paired-pulses interval: 100ms) were applied every 20 seconds. These pulses were generated by a stable stimulator. The stimulation intensity was progressively increased (1-10μA) until a large EPSC was obtained in an all-or-none manner.

For mGluR-LTD experiments (mice 2-3 months of age), cells were held at -60 mV and a patch pipette (1MΩ) filled with aCSF was placed in the molecular layer, in the vicinity of the PC, and moved until the PF response could be elicited with a minimal stimulus intensity. Two current pulses (0.2ms, paired-pulses interval: 100ms) were applied every 20 seconds. The stimulation intensity was chosen to obtain an EPSC with an amplitude of approximately 200 pA. A baseline was recorded for at least 10 min and when judged stable, the cell was switched to current-clamp mode (with no holding current applied) for the application of 50 μM (RS)-3,5-Dihydroxyphenylglycine (DHPG) for 10min. Cells were then switched back to voltage-clamp and the response to pair-pulse stimulation was recorded for at least 30 min.

Spontaneous mEPSC (mice 3-4 weeks of age) were pharmacologically isolated by bath application of 0.5 μM tetrodotoxin. The cells were held at -70 mV and spontaneous mEPSCs were recorded for at least 5min. A minimum recording duration of 2min was used for further analysis.

Erasmus Ladder Behavioral Assay. The basal motor function was analyzed using the fully automated Erasmus Ladder behavioral assay as described (10). Briefly, mice were trained to walk on the ladder for 72 consecutive runs per day during 4 days. The steptime, which is defined as the time needed to

place one of the front paws from one rung to the other, the number of mis-steps, defined as contact with the descended rungs, and the number of counted runs were recorded.

Statistical Analysis. Pairwise comparisons were performed using Student's t test. For multiple comparisons, two-way repeated measures analysis of variance (ANOVA) followed by post hoc Tukey test (HSD) was used. Cumulative probability distributions were analyzed by Kolmogorov-Smirnov test. Data are represented as the mean ± standard error of the mean (SEM)

References

1. K. F. Tanaka et al., Biol. Psychiatry 67, 770 (2010).
2. T. Zu et al., J. Neurosci. 24, 8853 (2004).
3. J. Y. Song, K. Ichtchenko, T. C. Sudhof, N. Brose, Proc. Natl. Acad. Sci. USA 96, 1100 (1999).
4. H. U. Zeilhofer et al., The Journal of Comparative Neurology 482, 123 (2005).
5. E. C. Budreck, P. Scheiffele, Eur. J. Neurosci. 26, 1738 (2007).
6. H. Taniguchi et al., J. Neurosci. 27, 2815 (2007).
7. J. M. Fritschy, H. Mohler, The Journal of Comparative Neurology 359, 154 (1995).
8. N. Sans et al., J. Neurosci. 23, 9367 (2003).
9. E. M. Schneider Gasser et al., Nature Protocols 1, 1887 (2006).
10. M. F. Vinueza Veloz et al., Genes Brain Behav. 11, 325 (2012).

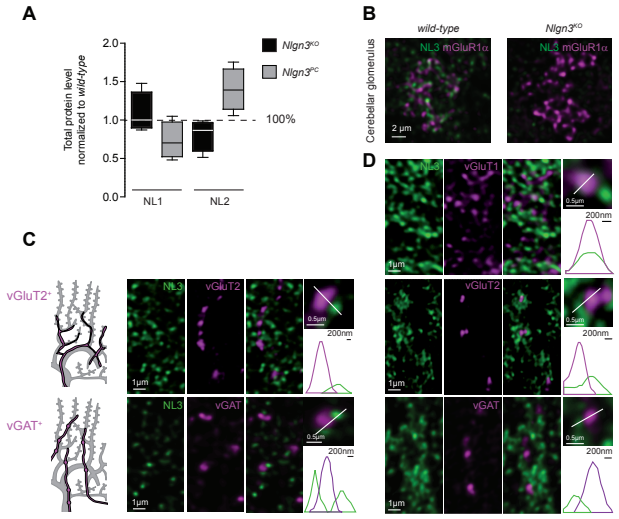

Fig. S1: NL3 synaptic localization

(A) Quantitative Western-Blot analysis reveals no change in NL1 and NL2 protein levels in Nlgn3^{KO} mice or Nlgn3^{PC} mice compared to wild-type mice (NL1: Nlgn3^{KO} 1.1 ± 0.1, Nlgn3^{PC} 0.7 ± 0.1; NL2: Nlgn3^{KO} 0.8 ± 0.1, Nlgn3^{PC} 1.4 ± 0.1; n ≥ 3 mice). (B) In the IGL, NL3 is localized at mGluR1^{+} mossy fiber terminals. NL3 antibody reactivity is largely abolished in Nlgn3^{KO} mice.
(C) On PCs, NL3 is not detected apposed to either vGluT2^{+} CFs or vGAT^{+} inhibitory terminals. The distance between the peak intensity of the respective markers and NL3 was higher than the optical resolution limit of 240nm indicating a lack of colocalization. (D) Selective association of NL3 with PF-synapses is also observed for NL3 selectively overexpressed in PCs (Nlgn3^{PC} mice).

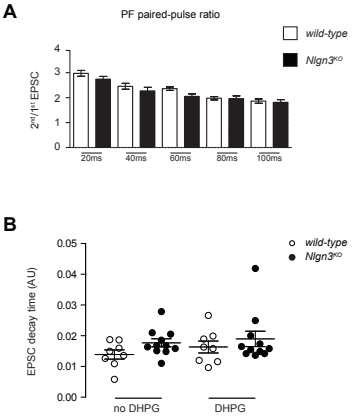

Fig. S2: PF EPSC paired-pulse ratio and decay time

(A) Analysis of the ratio between the second and the first PF mEPSC (paired-pulse ratio, PPR) reveals no difference between wild-type mice and Nlgn3^{KO} mice. (B) Analysis of the PF EPSC decay time before DHPG treatment reveals a trend towards an increase in Nlgn3^{KO} mice compared to wild-type (wild-type: 0.013 ± 0.001; Nlgn3KO: 0.017 ± 0.001; p = 0.07, unpaired t-test). After DHPG treatment decay times in both genotypes appear more similar (wild-type: 0.017 ± 0.002; Nlgn3KO: 0.019 ± 0.002).

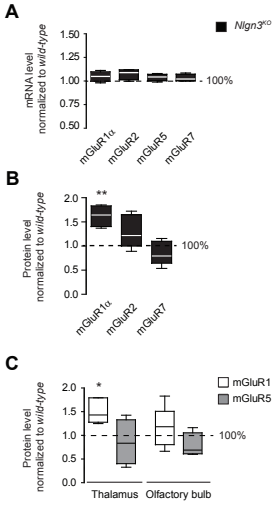

Fig.S3: Selective mGluR1a de-regulation in Nlgn3KO mice

(A) qPCR analysis reveals no difference between wild-type mice and Nlgn3KO mice in Grm1 (mGluR1), Grm2 (mGluR2), Grm5 (mGluR5) or Grm7 (mGluR7) mRNA level normalized to Gapdh ($n \geq 3$ mice).
(B) Quantitative western-blot analysis of cerebellar lysates reveals a specific increase in mGlur1α protein level in Nlgn3KO ($n \geq 4$, ** $p = 0.002$, t-test) but no significant change for mGluR2 (wild-type: 1.9 ± 0.2; Nlgn3KO: 2.5 ± 0.3; $n \geq 3$ mice) or mGluR7 (wild-type: 2 ± 0.3; Nlgn3KO: 1.7 ± 0.2; $n \geq 4$ mice).
(C) Quantitative western-blot analysis reveals that the mGluR1α de-regulation observed in $Nlgn3^{KO}$ is not restricted to the cerebellum but also observed in the thalamus (wild-type: $2,6 \pm 0.4$; $Nlgn3^{KO}$: 4 ± 0.3; $n \geq 5$ mice, *$p < 0.05$, t-test). No significant change was found in the olfactory bulb (wild-type: 0.5 ± 0.1; $Nlgn3^{KO}$: 0.6 ± 0.1; $n \geq 5$ mice) or for mGluR5 in the corresponding brain regions (thalamus: wild-type: 1.4 ± 0.2; $Nlgn3^{KO}$: 1.1 ± 0.3; $n \geq 4$ mice; olfactory bulb: wild-type: 0.9 ± 0.1; $Nlgn3^{KO}$: 0.7 ± 0.1; $n \geq 3$ mice).

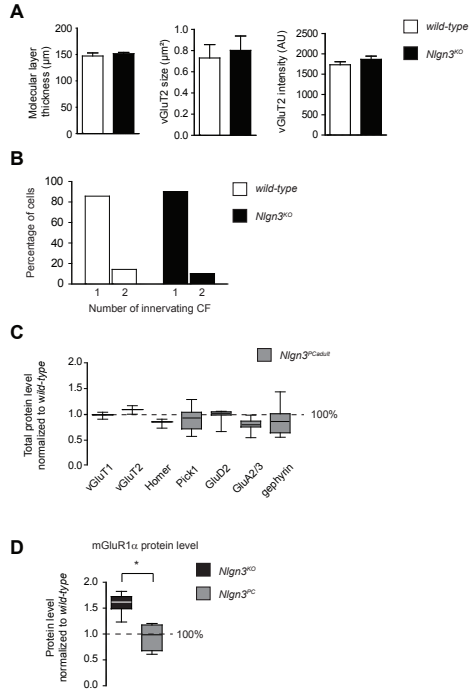

Fig. S4: Absence of vGluT2 morphology alteration and CF-PF multi innervation in Nlgn3KO mice

(A) Immunohistofluorescence analysis of the ML thickness in the straight portion of the lobule IV/V reveals no difference between wild-type mice and Nlgn3KO mice (wild type: $147 \pm 6\ \mu m$; Nlgn3KO: $151 \pm 2\ \mu m$; $n \geq 3$ mice). In the region of CF overshooting, both the size and the intensity of the vGluT2+ clusters remain similar between the two genotypes (size: wild type $0.7 \pm 0.09\ \mu m^2$; Nlgn3KO $0.8 \pm 0.1\ \mu m^2$; intensity: wild type: 1619 ± 30; Nlgn3KO: 1602 ± 30; $n \geq 3$ mice).
(B) Electrophysiological recordings reveal that the percentage of PC innervated by more than one CF is similar between wild-type mice and Nlgn3KO mice (wild-type: 12%; Nlgn3KO: 10%; $n \geq 8$ cells).
(C) Quantitative western-blot analysis on wild-type and Nlgn3PC cerebella shows that the re-expression of NL3 after completion of the neuronal development does not affect the protein level of general pre- and post-synaptic markers.
(D) The mGluR1α elevation is already detected in 3-4 weeks old animals. Increased mGluR1α levels are suppressed by constitutive NL3 re-expression in PC or late expression from P30-P60 (see Fig. 4F). The mGluR1α protein level was quantified by western-blot in P21 to P30 cerebella. We found an increase in Nlgn3KO mice which can be reversed by a Purkinje cell specific re-expression of NL3 (wild-type: 3 ± 0.5; Nlgn3KO: $4,8 \pm 0.2$; Nlgn3PC: $2,8 \pm 0.4$; $n \geq 4$ cells; *$p < 0.05$).